1D - 0D models to study the effect of atrial fibrillation on coronary circulation

Virginia Clemente

[a]*Università Campus Bio-Medico di Roma, Via Álvaro del Portillo, 21, Rome, 00128, Italy*

Abstract

Multiscale modelling is a promising instrument for the study of coronary haemodynamics. In the following review, it is analysed a validated multiscale model of the left coronary circulation using high-fidelity data from nine adult sheep. Thereafter, it is investigated the effect of ventricular rate during atrial fibrillation (AF) on coronary perfusion using an open model that includes the entire left heart arterial tree. All calculated haemodynamic parameters are based on the left anterior descending artery (LAD), taking into account the waveform, amplitude and perfusion of the coronary blood flow. Finally, it is considered a closed-loop model, taking into account the four cardiac chambers and closing the loop with the pulmonary circulation, to perform an inter-layer and inter-frequency analysis focusing on the ratio of mean beat-to-beat blood flow in AF versus sinus rhythm (SR).

Keywords: Atrial Fibrillation, Coronary Circulation, Models, Multi-scale Models, Application, Coronary Perfusion

1. Introduction

By combining numerical techniques and mathematical modelling of different orders and geometric detail, computational haemodynamics is becoming a powerful tool in translational medicine to accurately reproduce the human cardiovascular system [26, 34]. The computational approach allows the analysis of haemodynamic variables that are difficult to measure, the understanding of physiological and pathological mechanisms, the simulation of haemodynamic responses induced by medical procedures (e.g. drug administration and surgery), the monitoring of the onset and progression of cardiovascular diseases and the generation of patient-specific indications. In particular, in this review the focus will be on the modelling of the coronary circulation in the presence of atrial fibrillation (AF). AF is the most common sustained arrhythmia and is associated with significant mortality and morbidity from stroke, thromboembolism, heart failure and reduced quality of life. With the ageing of the population in developed countries and improvements in the management of myocardial infarction and heart failure, the prevalence of AF is increasing significantly. Its prevalence has been steadily increasing over the past decades, with a threefold increase over the past 50 years [30], and recent epidemiological projections predict a further increase, with an estimated 16-17 million prevalent cases in the US and Europe by 2050 [16]. Given this significant epidemiological burden, a detailed understanding of the physiopathology of this arrhythmia is warranted.

Atrial fibrillation causes several disabling symptoms such as palpitations, low blood pressure, reduced exercise tolerance and pulmonary congestion. In addition, AF patients may complain of angina-like chest pain and symptoms due to alterations in myocardial perfusion and transient myocardial ischaemia, even in the absence of significant coronary artery disease (CAD)[14]. The reciprocal effects between AF and coronary perfusion impairment have long been discussed. Indeed, clinical studies suggest that AF promotes coronary flow impairment [18] and a mismatch between coronary blood flow and myocardial metabolic demand [14]. Even in the absence of significant CAD, AF can worsen subendocardial perfusion during diastole. As CAD and AF often coexist and share several risk factors, the clinical literature usually considers the coexistence of both pathologies [19].

Thus, computational haemodynamics can be a valuable tool in clinical applications. Recently, coronary blood flow has been modelled with approaches ranging from full 3D coupled with electromechanical response to lower order multiscale models [17]. Among the different approaches, our focus on 0D-1D models is motivated by the fact that these multiscale models guarantee a very good compromise between computational cost, level of haemodynamic detail and reliability of results [31]. Indeed, the focus of this review is on the effects of AF on the coronary circulation, and for this reason this type of model is appropriate.

In section 2, we describe a multiscale coronary circulation model in which an anatomically based 1D network accounts for wave propagation effects in the main conduit arteries, and numerous 0D compartments inserted throughout the network represent microvascular impedance and established sources of intramyocardial pressure. Based on the validated multiscale model of section 2 and combined with modelling of the heart and arterial tree, in section 3 we will look at a computational approach to investigate to what extent coronary perfusion is impaired in AF and how it correlates with ventricular rate. Finally, in section 4, we will go into a deeper understanding of the coronary perfusion of the different layers of the myocardium during AF.

2. Multiscale numerical model of the left coronary circulation and in vivo validation

Mynard et al. (2014) [23] proposed a classical, anatomically based and very detailed one-dimensional (1D) network of the major conduit arteries and a lumped parameter model (0D) of microvascular beds downstream of each 1D coronary artery. A key strength of this approach is that it accounts for microvascular properties and extravascular forces that differ regionally and transmurally, as well as wave propagation effects in the conduit arteries. They validated a multiscale model of the left coronary circulation using high-fidelity data from nine adult sheep. These models are validated on two levels: a general validation of microcirculatory flow patterns against published data, and a subject-specific validation utilizing high fidelity in vivo measurements of proximal circumflex (Cx) coronary arterial flow.

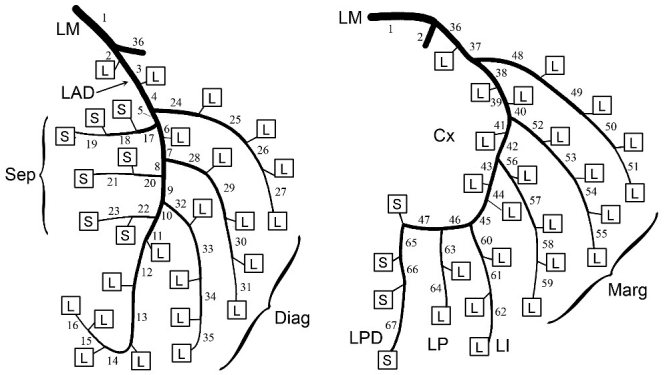

Figure 1: Schematic of the 1D model of left coronary arteries. The 1D segments terminate in instances of the 0D intramyocardial model that supply the left ventricular free wall (L) or ventricular septum (S; Sep). Cx, circumflex; Diag, diagonal; Marg, marginal; LAD, left anterior descending; LI, left inferior; LM, left main; LP, left posterior; LPD, left posterior descending. [23]

2.1. 1D model of conduit coronary arteries

Based on the gross similarity between left dominant anatomies in humans and sheep [6], the 1D conduit artery model shown in Figure 1 was adapted from measurements in humans by Dodge et al. [4]. Following Olufsen [25], stiffness of the 1D segments was determined by a prescribed reference wave speed (c_0), calculated as a function of reference radius (r_0),

$$c_0^2 = \frac{2}{3\rho}[k_1 exp(k_2 r_0) + k_3] \tag{1}$$

where the values of the coefficient were taken from [46] and are $k_1 = 2 * 10^7 gs^{-2}cm^{-1}$; $k_2 = -22.53cm^{-1}$; $k_3 = 8.65 * 10^5 gs^{-2}cm^{-1}$.

The 1D modeling methodology has been described in detail in [21, 22]. Briefly, the nonlinear 1D equations governing pressure (p), cross-sectional mean velocity (u) and cross-sectional area (A) are:

$$\frac{\partial A}{\partial t} + \frac{\partial (Au)}{\partial x} = 0 \tag{2}$$

$$\frac{\partial u}{\partial t} + u\frac{\partial u}{\partial x} + \frac{1}{\rho}\frac{\partial p}{\partial x} = -\frac{\xi \pi \mu}{\rho}\frac{u}{A} \tag{3}$$

where $\rho = 1.06\frac{g}{cm^3}$ is blood density and $\mu = 0.035 poise$ is blood viscosity. The viscous term incorporates the constant ξ and for a Poiseuille velocity profile they use $\xi = 22$, following [32], which better reflects the physiological velocity profile. The following physiologically relevant pressure-area relation was used:

$$p - p_{ext} = \frac{2\rho c_0^2}{b}\left[\left(\frac{A}{A_0}\right)^{\frac{b}{2}} - 1\right] + \frac{\Gamma}{A\sqrt{A}}\frac{\partial A}{\partial t} + p_0 \tag{4}$$

where A_0 is reference area, p_0 is pressure and b is a constant governing the shape of the pressure-area relation, estimated via a nominal zero-area pressure of $10 mmHg$ [20].

The viscoelasticity constant, Γ is difficult to estimate and is assumed to be zero for the main results; however, about the effect of viscoelasticity in the sensitivity analysis, they assumed $\Gamma = 1,792 r_0 + 1,522 \frac{g}{s}$, as in Alastruey et al. [1]. External pressure (p_{ext}) was set to zero for epicardial conduit arteries, but for septal conduit arteries that lie within the contracting ventricular septum, p_{ext} was set to the average of left ventricular (LV) and right ventricular (RV) cavity pressures (p_{LV} and p_{RV}),with an assumed p_{RV} of 0.2 pLV [22]. The 1D governing equations were solved using a finite element method [21], with continuity of total pressure ($p + \frac{1}{2}\rho u^2$) applied at vessel bifurcations. The viscoelastic term in 4 was treated with an operator splitting technique as described elsewhere [5].

2.2. 0D model of intramyocardial vascular beds

In the coronary circulation, blood flow is delivered to the microvasculature via penetrating arteries that branch off the main conduit arteries, as shown in Fig. 2. The interface between 1D and 0D in this model was at the level of these penetrating arteries. Short 1D penetrating artery segments were inserted throughout the 1D model and were coupled to the 0D model instances (depicted as boxes in Fig. 1) via a penetrating artery characteristic impedance and compliance (Z_{pa} and C_{pa}, Fig. 2). On the venous side, a penetrating vein characteristic impedance and compliance (Z_{pv} and C_{pv}) were connected to an assumed constant right atrial pressure ($p_{RA} = 5 mmHg$).

The microvascular model was divided into **subepicardial**, **midwall**, and **subendocardial** layers, how it can see in Fig.2

Following Spaan et al. [33], each layer consisted of two compartments, whose volume varied according to the compliances C_1 and C_2. The compartments each contained a resistance (R_1 and R_2), while a "middle" resistance R_m was shared by both compartments, keeping in mind that the physical portion of the microvasculature represented by the two compartments is uncertain and probably changes with perfusion pressure.

Instantaneous compartment volume was given by

$$V_i(t) = V_{0,i} + \int_0^t C_i \frac{dp_{tm,i}}{dt'}\, dt' \tag{5}$$

where $i = \{1, 2\}$ and transmural pressure (p_{tm}) is equal to intravascular pressure (p) minus intramyocardial pressure (p_{im},

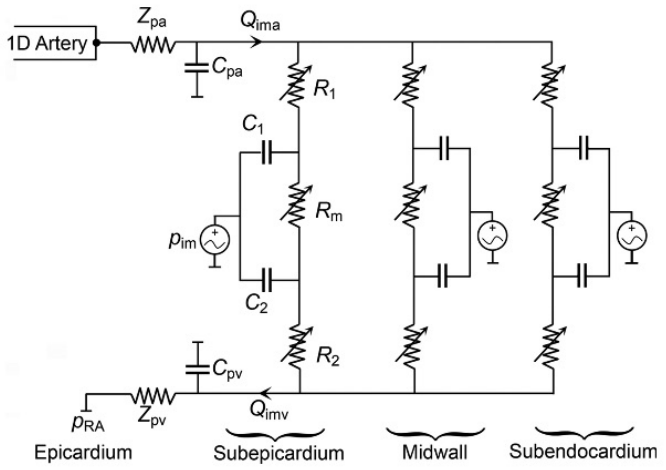

Figure 2: Coronary microvascular model. The model is divided into three transmural layers (subendocardium, midwall, and subepcardium), each containing 2 compartments (with compliances, resistances, and a shared middle resistance R_m) acted on by intramyocardial pressure (p_{im}). Each instance of the model is coupled to a 1D artery via a penetrating artery characteristic impedance (Z_{pa}) and compliance (C_{pa}), while venous counterparts (Z_{pv} and C_{pv}) connect to right atrial pressure (p_{RA}). Q_{ima} and Q_{imv} are the total intramyocardial arterial and venous flows, respectively [23]

Fig. 2). Based on Poiseuille's law, the assumed volume-resistance relationship [3] was

$$R_1 = R_{0,i}\frac{V_{0,i}^2}{V_i^2} \tag{6}$$

where $R_{0,i}$ is a reference resistance corresponding to a reference volume $V_{0,i}$. The middle resistance shares volume from the two compartments as follows,

$$R_m = R_{0,m}\left[\gamma\frac{V_{0,1}^2}{V_1^2} + (1-\gamma)\frac{V_{0,2}^2}{V_2^2}\right] \tag{7}$$

where γ is a constant between 0 and 1.

Intramyocardical pressure, p_{im}, can be best accounted for by a combination of two mechanisms (Algranati et al. [2]):

- The first is cavity-induced extracellular pressure (p_{CEP}), which arises from transmission of ventricular cavity pressure into the heart muscle.
- The second mechanism is shortening-induced intracellular pressure (p_{SIP}).

They therefore assumed that p_{im} is given by

$$p_{im} = \alpha p_{CEP} + p_{SIP} \tag{8}$$

Given the findings of Algranati et al. [2] that the combination of p_{CEP} and p_{SIP} are best able to account for current experimental data, in the present study they assume $\alpha = 1$. p_{CEP} for the LV free wall was assumed to vary linearly from cavity pressure at the endocardium to pericardial pressure (here assumed to be atmospheric pressure) at the epicardium. While they assumed that p_{SIP} is directly proportional to ventricular chamber elastance. They assumed that p_{SIP} is directly proportional to ventricular chamber elastance

$$p_{SIP} = \varphi E_{LV} \tag{9}$$

2.3. Validation procedure

Validation of the multiscale coronary model was performed with minimal data fitting. They assumed a proximal C_x wave speed of $9.0m/s$ in all animals. Measured subject-specific aortic pressure was prescribed at the inlet of the left main coronary artery, having applied a delay of $15ms$ to account for the estimated delay between pressure generation in the myocardium and p_{LV} sensing just below the mitral valve, caused by a ventricular wave speed of $\approx 4m/s$.

Individually measured p_{LV} was used directly for p_{CEP}. To estimate p_{SIP}, LV cavity volume was derived by integrating measured aortic flow and assuming an ejection fraction of 0.68 [13] and then calculating chamber elastance as the ratio of cavity pressure and volume. It was considered only one free parameter, total intramyocardial resistance, which was uniformly adjusted using an iterative beat-to-beat algorithm to achieve measured mean flow in the proximal Cx. All other parameters described before were treated as subject generic.

*Statistical analysis.*Comparisons of experiment vs. simulation data were performed with repeated measures ANOVA. Significance was defined as $P < 0.05$.

2.4. Results

This study has validated a multiscale model of the left coronary circulation using high-fidelity measurements in adult sheep. Agreement between simulated and measured Cx flow waveforms was excellent in most cases, suggesting that the model adequately captured the most important mechanisms underlying the coronary flow waveform.

2.4.1. Model Validation

Employing minimal data fitting, it is validated a multiscale model on two levels.

For a general validation, it is showed that characteristic flow patterns throughout the model were representative of published in vivo data. Thus simulated small artery flow exhibited some retrograde flow during early systole, near zero flow during the remainder of systole, and a dominance of forward flow in diastole; conversely, venous flow was predominantly systolic (Fig. 3A). Sustained retrograde flow occurred during systole in the subendocardium as has been observed in vivo; in some cases, experimentally measured subendocardial flow has been near zero during the latter part of systole as in the midwall layer of our model (Fig. 3B). Almost all midwall flow occurred during diastole, while subepicardial flow had a similar (antegrade) magnitude in systole and diastole. Transmural flow patterns on the venous side were all systolic-dominant, with notable forward diastolic flow in the subepicardial layer only (Fig. 3C). Vascular volume varied most in the subendocardium (arterial 17%; venous 7%) and least in the subepicardium (arterial 1.6%, venous 2.3%; Fig. 3D, data shown only for arterial side).

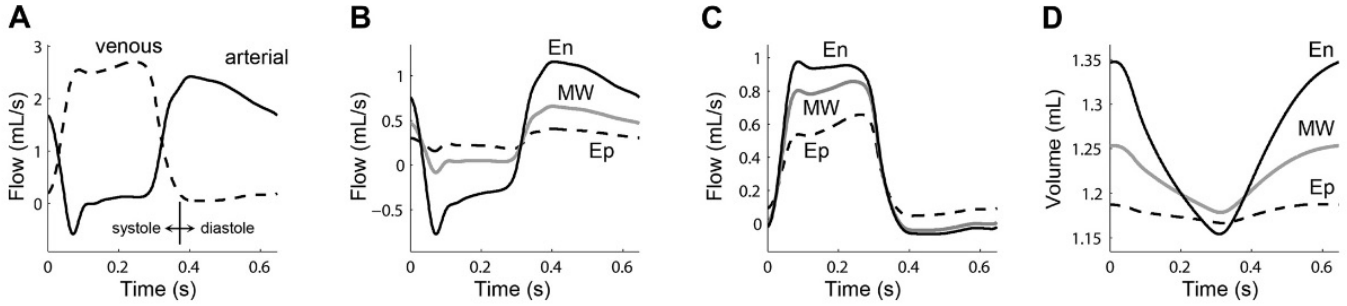

Figure 3: Comparison of total microvascular arterial vs. venous flow (A), total flow in the subendocardium (En), midwall (MW), and subepicardium (Ep) on the arterial side (B) and venous side (C), and total vascular volume variations in the arterial compartment for the three transmural layers (D).[23]

For subject-specific validation, measured LV pressure, aortic pressure and flow, and LV weight from a particular subject were used as model inputs. Mean Cx flow was matched to the subject by adjusting total coronary resistance. In 9 adult sheep, the agreement between simulated and in vivo flow waveforms was excellent in most cases. Overall levels of systolic and diastolic flow were similar in the model and experiments, although late systolic flow was underestimated in some cases.

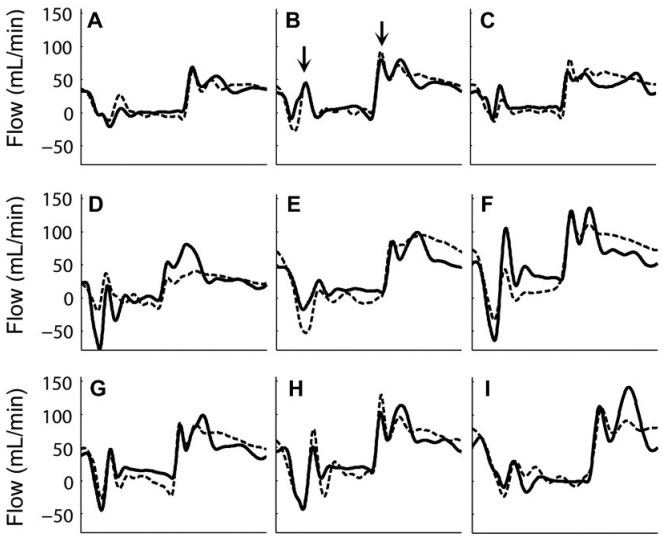

Figure 4: A–I: comparison of measured (solid lines) and simulated (dashed lines) proximal circumflex coronary arterial flow waveforms in 9 adult sheep. [23]

Figure 4 compare model and experimental flow waveforms in the proximal Cx of adult sheep. The waveforms were grossly similar to the diastolic-dominant microvascular arterial waveform (Fig. 3A) but with superimposed oscillatory flow transients during early systole and early diastole (arrows in Fig. 4). Visual agreement between model and experimental waveforms was excellent in most cases, with the model generally performing well in capturing both the flow transients and the levels of systolic and diastolic flow. The root mean square error, normalized to maximal flow, was 16.7 ± 4.9% (range 12.4 to 27.0%). In some cases, late systolic flow was underestimated (Fig. 4E-G,) or the amplitude of the early systolic flow transient was underestimated (Fig. 4,D and F). There was no difference in the duration of the key phases of the flow waveform (S1-early systole, S2-late systole, D1-early diastole, and D2-late diastole) between model and experiment. The model underestimated S2 flow for adults ($P < 0.05$).

2.4.2. Sensitivity analysis

Due to the large number of model parameters, a comprehensive sensitivity analysis was not possible. They included only those global parameters whose values were approximated on the basis of relatively loose constraints (Fig. 5). Wave speed appeared to be the most important parameter governing the early systolic and early diastolic flow transients, which supports the view that these features mainly arise from wave propagation effects; hence, 1D segment lengths would also be expected to influence these features. The magnitude of p_{SIP} had a substantial influence on overall systolic flow; although not included in the analysis, p_{CEP} would clearly also have a large influence on systolic flow. The aortic pressure shift, wave speed and Cpa were all important determinants of a late systolic negative flow spike. Other parameters had a relatively minor effect on the flow waveform.

A model sensitivity analysis suggested that:

- early systolic/diastolic flow transients are primarily governed by wave speed of the main conduit arteries,
- p_{SIP} provides a substantial contribution to systolic flow impediment and should be combined with p_{CEP} in modeling studies.

2.5. Integration of the previous model with the Cardiovascular System

In a later paper in 2015 by Mynard et al. [24], the coronary modelling considered only the main coronary arteries and branches, was extended to the right coronary circulation and coronary veins, and finally incorporated into a 0D-1D model of the entire adult circulation. The coronary vascular bed model is identical to that in [23] and consists of three myocardial layers, each containing two compliant compartments (C_1, C_2). Three non-linear resistances (R_1, R_m, R_2) in each layer are dependent on blood volume in the two compartments via Eq. 5,6,7. The compliances are subjected to p_{im}, calculated as the sum of p_{CEP}

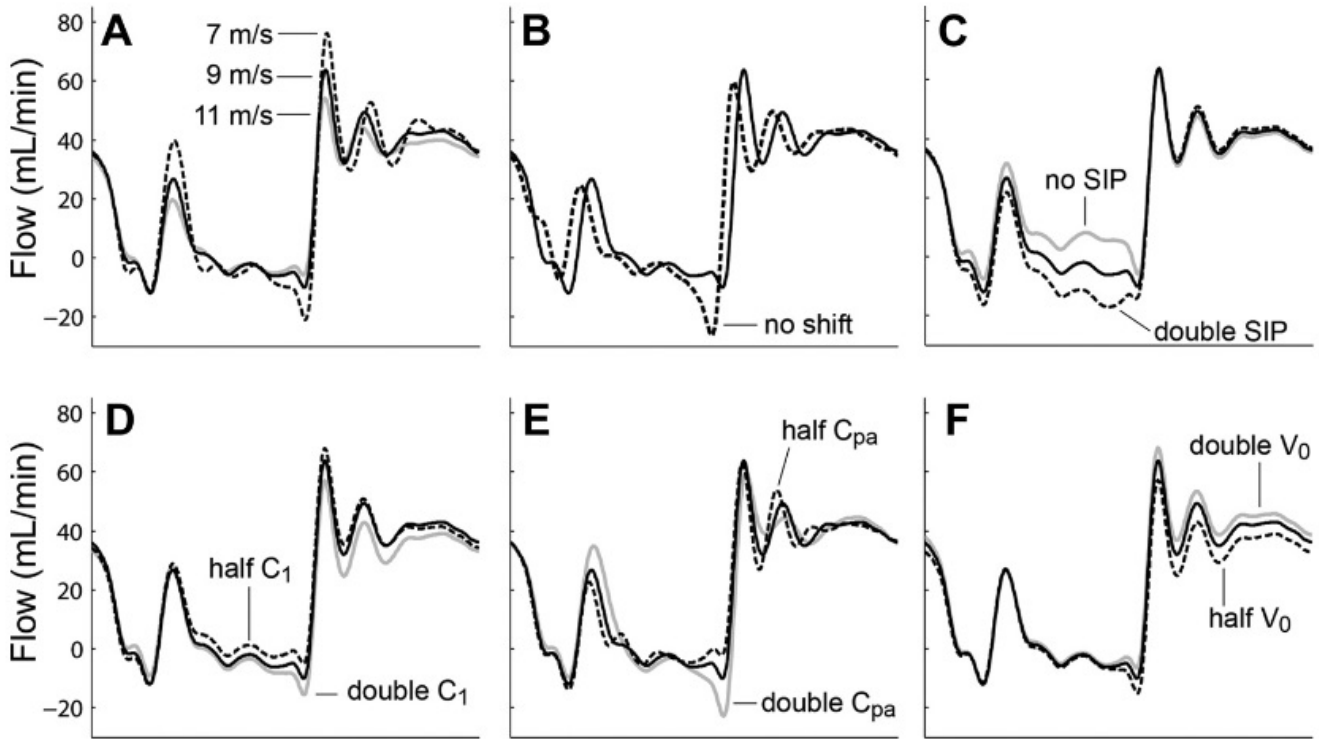

Figure 5: Sensitivity of simulated proximal circumflex coronary arterial flow waveforms to changes in wave speed (A; all 1D segments increased/decreased by 22%, values shown are for the proximal circumflex); shift applied to the input aortic pressure (B); SIP (C); microvascular compliance C1 (D; see Fig. 2); penetrating arterial compliance C_{pa} (E; 2); and microvascular reference volume, V_0 (F) [23].

and p_{SIP} [2]. p_{SIP} is assumed to be directly proportional to effective ventricular chamber elastance, that is,

$$p_{SIP} = \alpha_{SIP}\left[\frac{p_v}{v_v - V_{p=0,V}}\right] \tag{10}$$

where α_{SIP} is a constant and V subscripts refer to the left ventricular cavity for the left ventricular free wall and septal myocardium, and the right ventricular cavity for the right ventricular free wall. The model is coupled to a terminal 1D artery and vein via penetrating artery/vein characteristic impedances and compliances. The aim was to present and validate in vivo a coronary model capable of describing regionally and transmurally different microvascular properties and wave propagation effects in the conduit arteries. The authors were able to quantify forward and backward wave intensity and the interaction between cardiac function/mechanics and wave dynamics.

3. Impaired coronary blood flow at higher HR during AF

Scarsoglio et al. (2019) [28] proposed a computational approach, based on a validated multiscale model, to investigate to what extent coronary perfusion is impaired in AF and how this relates to the ventricular rate. Recent clinical studies suggest that AF promotes an impairment of the coronary flow [18] and a mismatch of coronary blood flow and myocardial metabolic demand [14].

3.1. Methods

The proposed computational approach can be sketched as a three-steps algorithm: RR beating extraction, 0D-1D cardiovascular modelling resolution, coronary perfusion evaluation. The three phases are schematically represented as overall flow chart of the stochastic modelling approach in Fig. 6.

3.1.1. RR beating features

RR [s] is defined as the cardiac beating period, with the heart rate, $HR = \frac{60}{RR}$. They use artificially built RR intervals to avoid the patient-specific details. RR intervals during AF are described by the superposition of two independent times, $RR = \varphi + \eta$. φ is taken from a Gaussian distribution and the extraction relies on the correlated pink noise, while η is taken from an Exponential distribution and the extraction is based on the uncorrelated white noise. The resulting RR is thus represented by an exponentially modified Gaussian distribution, which is the most common distribution during AF [12][29]. AF is simulated at different ventricular rates from 50 to 130 [bpm].

3.1.2. Mathematical Modelling

sThe present study relies on the multiscale model proposed by Guala et al. [11], which combines the 0D-1D modelling of the left heart and arterial tree [9, 10, 29] together with the coronary circulation model as introduced by Mynard et al. [23, 24]. The geometrical domain includes the arterial tree, the left heart, with mitral and aortic valves, and the left coronary circulation.

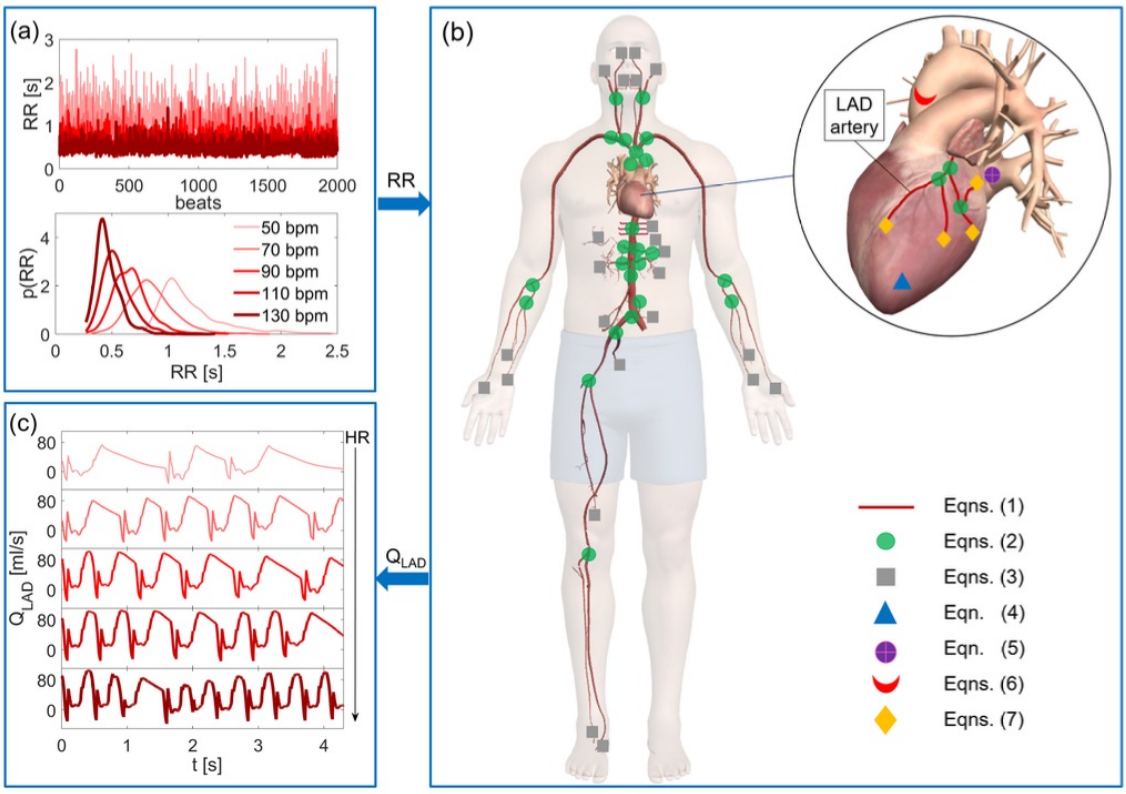

Figure 6: Flow chart of the computational algorithm. (a) RR beating. 2000 RR beats extracted in AF at the selected HR (50, 70, 90, 110, 130 bpm) and the corresponding probability distribution functions. (b) Schematic representation of the 0D-1D cardiovascular model, together with the cor- responding governing equations of each district. (c) Examples of the resulting QLAD time-series at different HRs.The Eqns in the picture can be found in [28].

Figure 6b shows a schematic representation of the cardiovascular model, together with the corresponding governing equations of each district. Regarding the arterial tree, the systemic arterial circulation consists of 48 large-medium arteries and 24 distal groups. The large-medium arteries are described through the 1D form of the mass and momentum equations, in terms of pressure, section area, and flow rate, while the distal group consist of three-element Windkessel submodels. The left heart is described through a time - varying elestance model. The left coronary circulation originates from the aortic root and includes 7 large-medium arteries, which are modelled as the systemic arterial tree. Each artery ends up with a microvascular distal district. Each coronary distal group is ruled by the following system, using all parameters set as in [23, 24].

$$\begin{cases} C_{1j}\frac{dP_{1j}}{dt} = C_{1j}\frac{dP_j^{im}}{dt} + \frac{P_a - P_{1j}}{R_{ij}} - \frac{P_{1j}-P_{2j}}{R_{2j}}, j = 1, ..., 3, \\ C_{2j}\frac{dP_{2j}}{dt} = C_{2j}\frac{dP_j^{im}}{dt} + \frac{P_{1j}-P_{2j}}{R_{2j}} - \frac{P_{2j}-P_v}{R_{3j}}, j = 1, ..., 3, \\ C_{pa}\frac{dP_a}{dt} = \frac{P_{in}-P_a}{Z_{pa}} - \sum_{j=1}^{3}\frac{P_a - P_{1j}}{R_{ij}}, \\ C_{pv}\frac{dP_v}{dt} = \sum_{j=1}^{3}\frac{P_{2j}-P_v}{R_{3j}} - \frac{P_v - P_o ut}{Z_{pv}}, \end{cases} \tag{11}$$

3.1.3. Hemodynamic parameters for coronary perfusion

They introduce the hemodynamic parameters used to quantify coronary blood flow variations at different HRs during AF, that are computed based on the left anterior descending (LAD) artery, which is the most important vessel in terms of myocardial blood supply (see Fig. 6c). By dividing the RR interval into systolic, RR_{sys}, and diastolic, RR_{dia}, they can define V_{sys}, as the volume of blood flowing through the LAD artery during systole and V_{dia} related to diastole

$$V_{sys} = \int_{RR_{sys}} Q_{LAD}(t)dt, \tag{12}$$

$$V_{dia} = \int_{RR_{dia}} Q_{LAD}(t)dt, \tag{13}$$

where Q_{LAD} is the flow rate signal in the LAD artery. The combination of the two volume gives the net flow through the LAD artery, $SV = V_{sys} + V_{dia}$. By means of SV, the coronary blood flow per beat is expressed as $CBF = SVxHR$ [ml/min] instead of [ml/beat], giving a measure of myocardial perfusion and oxygen supply. To better compare the different HRs, they define the average behaviour of the LAD flow rate per beat over N cardiac periods

$$< Q_{LAD} >= \frac{1}{N}\sum_{i=1}^{N} Q_{LAD_i}(\tau) \tag{14}$$

where here $N = 2000$, Q_{LAD_i} is the Q_{LAD} of the i-th heartbeat, while $\tau = \frac{t}{RR_i}$ is the non-dimensional temporal coordinate. They also introduce the coronary perfusion pressure, $CPP = P_{dia} - P_{lved}$, where P_{dia} is the diastolic aortic pressure, while P_{lved} is the end-diastolic left-ventricular pressure.

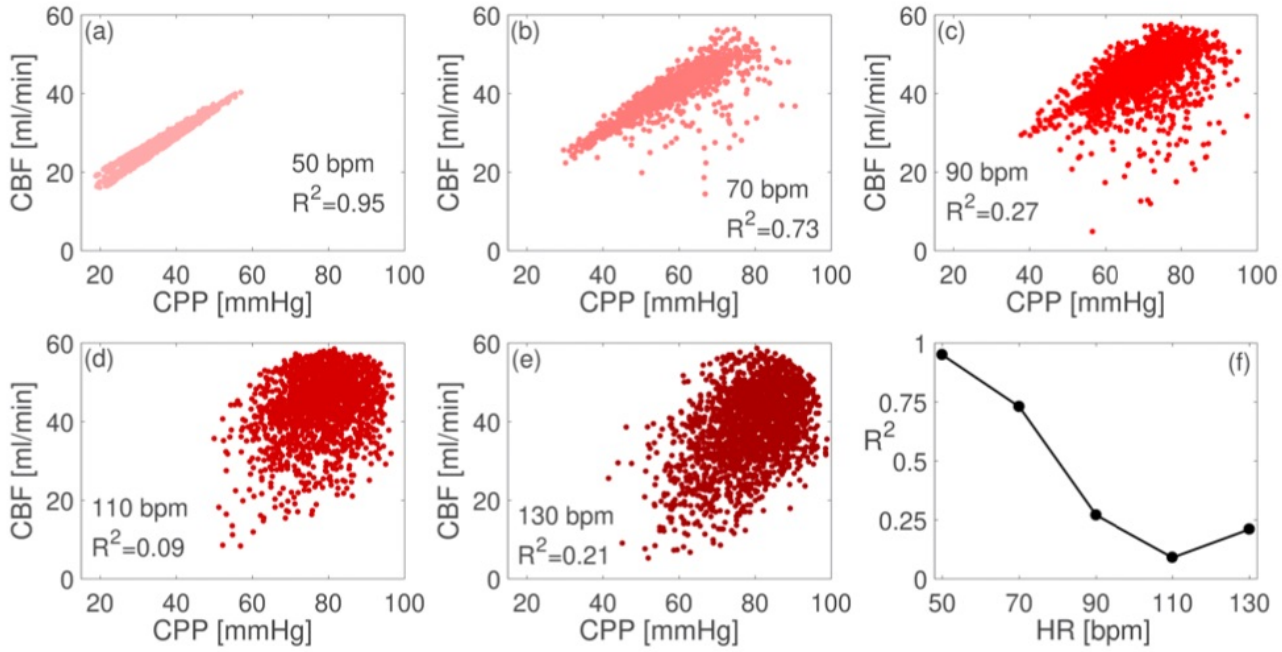

Figure 7: Coronary blood flow (CBF) as function of the coronary perfusion pressure (CPP) over 2000 cardiac cycles for $HR = 50, 70, 90, 110, 130$ bpm (panels from a to e). Panel f shows the coefficient of determination, R^2, for the relation CBF(CPP) as function of HR. [28]

In the end, to evaluate the myocardial oxygen supply-demand ratio, they compute the rate pressure product, $RPP = P_{sys} \times HR$ [mmHg/min], which is an estimate of the oxygen consumption.

3.2. Results

The results of this study shows that higher ventricular rate during AF exerts impaired coronary blood flow. In details, the combined effects of both AF and HR variations leads to the following results.

Waveform and amplitude of the coronary blood flow rate are deeply modified by increasing HR, with a substantial delay of the diastolic peak and a consequent flow rate reduction.

Fig. 8 shows that increasing HR the average, waveform is deeply modified. During both systole and diastole, at higher HRs the $< QLAD >$ signal is remarkably stretched forward in time with respect to lower HRs. As for the diastole, the typical behaviour revealed at lower HRs with a rapid growth, a maximum peak and a slow decrease, is completely lost at higher HRs. This because, at higher HR, the diastole length is much more reduced than systole. Therefore, for $HR > 90bpm$ $< QLAD >$ changes its typical features: the diastolic growth of $< QLAD >$ is much slower, so that the maximum peak is reached towards the end of the beat, without even facing the decreasing phase. As a consequence, at higher HRs the next systolic phase starts with much higher $< QLAD >$ values.

Mean values of the maxima grow with HR: the $Q_{max,sys}$ has a +78% increase from 50 to 130bpm, while$Q_{max,dia}$ increases by +21%, presenting a maximum value around 110 bpm. The growth of Q_{min} in average is instead much less pronounced, i.e. +6%.

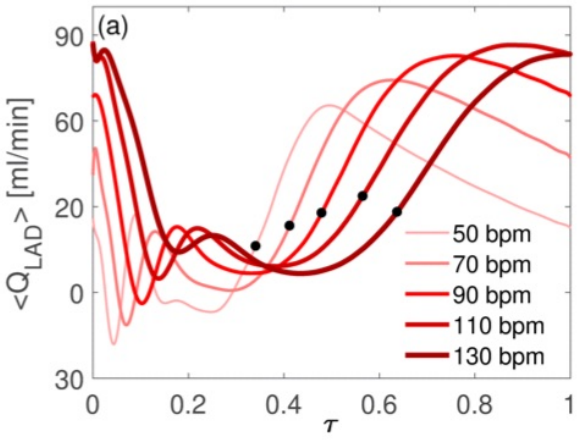

Figure 8: $< Q_{LAD} >$ at different HRs as function of the non-dimensional time, τ. Black dots indicate the beginning of the diastole.[28]

As a consequence of waveform variations,a sharp V_{dia} decrease and a slight V_{sys} increase in absolute terms occur, this involves a reduction in SV. However, the V_{dia} decrease does not proportionally scales with HR, but is slower for lower HR and faster for higher HR.

This results in a non-monotonic behaviour of CBF, which shows a maximum around 90-110 bpm: the slight diastole reduction does not promote consistent SV reduction, thus CBF overall grows between 50 and 90 bpm. Only beyond 90-110 bpm, the reduced diastole length makes SV, and therefore CBF, rapidly decrease. In terms of myocardial oxygen supply and demand, both CBF and RPP increase with HR up to 90 bpm. Once 90 bpm is exceeded, the oxygen demand still grows with

HR, while CBF reaches an optimal value and then decreases. This trend implies that, up to 90 bpm, the coronary perfusion increases trying to supply the increased myocardial oxygen demand. Beyond 90-110 bpm, instead, there is a progressive coronary impairment and a consequent imbalanced oxygen supply-demand ratio.

To further inquire into the irregularity induced by AF, whether coronary perfusion is differently affected by AF variability for increasing HR. To this end, dispersion plots of CBF as function of CPP are proposed in Fig. 7, at different HRs (panels from a to e). Unlike normal sinus rhythm, where CBF is derived from CPP, because positively correlated [15]; in AF, they observe that a strong linear correlation between CBF and CPP is still present at lower HR (Fig. 7, panels a and b), while it drops at higher HR (panels c to e). Therefore CBF positively correlates with CPP up to 70 bpm, but for higher HR the correlation dramatically drops towards zero and data become sparse. Fig. 7f displays the coefficient of determination, R^2, as function of the HR, revealing that for $HR \geq 90$ bpm CPP is no longer a good index to approximate the coronary blood flow.

At the end, the present computational framework focuses on the effects that different ventricular rates exert on the coronary circle during AF. Regardless of baseline clinical features, the present model suggests clinically relevant interpretations. In fact, higher ventricular rates during AF related to worse oxygen demand-supply ratio, indicating that not only the irregularity of the rhythm, but even the ventricular response in AF, may play a significant role in impairing coronary blood flow.

4. AF effects on coronary perfusion across different myocardial layers

Saglietto et al. (2022) [27] used an advanced computational model of the human cardiovascular system, including both arterial and venous vascular compartments, cardio-pulmonary circulation and short-term autoregulation mechanisms, with the aim to deepen comprehension of coronary perfusion of the different layers of the myocardium during AF. The model was employed to inquire into coronary hemodynamics during physiological (sinus) heart rhythm (SR) and AF. They focused on three mean ventricular rates: 75, 100 and 125 bpm, which were externally imposed as inputs of the present model. To allow proper comparison between SR and AF, the model assumes resting conditions (i.e., not exercise), thus the simulations reproduce AF with variable ventricular response and SR/tachycardic right atrial pacing in non-exercising patients.

4.1. Methods

Numerical simulations were carried out by means of a closed loop 1D-0D multiscale model of the entire human cardiovascular system, that merges the cardiovascular description as adopted in with the [8, 7] coronary modeling presented in [23, 24].

The model is composed by a 1D representation of the arterial tree, from the aortic valve to the peripheral circulation, through bifurcations and branches (Fig. 9). The mathematical description of the arterial model is based on the 1D Navier-Stokes equations for mass and momentum balance. The hemodynamic variables involved are the vessel lumen area A, and blood flow rate Q. Boundary conditions at the aortic inlet and onto each terminal branch section derive from the adjacent 0D models, whereas at arterial bifurcations mass and total pressure conservation are imposed. The four heart chambers are contractile and modeled as separate lumped parameter compartments via a time varying elastance approach. Cardiac valves are accurately described accounting for geometric, inertial, viscous and downstream vortex effects.

The model also includes a short-term baroreflex control mechanism accounting for the inotropic effect of both ventricles, as well as the control of the systemic vasculature.

Multiscale coronary arteries and microvasculature were modeled as proposed by Mynard and Smolich [24]. The main coronary arteries (numbered 49–62 in Fig.9) were treated as 1D vessels. Each 1D coronary artery terminates with a lumped parameter model of the downstream penetrating vasculature and microcirculatory districts. Such circuital representation provides a distinctive identification of the vasculature perfusing each myocardial layer, from the subepicardial (EPI), through the intermediate midwall (MID), up to the subendocardial (ENDO) circulation. These may further be subdivided in an arterial, an intermediate and a venous compartment. Resistances attributed to each myocardial layer are non-linear, depending on the current blood volume of the vessel, according to Poiseuille's law. Compliances allow for communication between intravascular and extravascular environment. The coronary loop is finally closed by connecting directly to the right atrium.

The RR beating extraction procedure is described in our previous works [29].

They focused on the microcirculatory districts representing the natural termination of the 1D epicardial arteries: vessel 57 for the LAD, vessel 53 for the Left Circumflex Artery (LCx), and vessel 61 for the Right Coronary Artery (RCA), as shown in Fig. 9. Attention was primarily addressed to the coronary arterial blood flow time series $Q(t)$ pertaining to each myocardial layer (EPI, MID and ENDO) under both sinus and fibrillated rhythm (subscripts SR and AF, respectively). For a generic myocardial layer and ventricular rate, beat-to-beat averaged distributions $Q_{SR,b}$ and $Q_{AF,b}$ were computed by averaging time series over each cardiac cycle:

$$Q_{SR,b} = \frac{1}{RR_{SR,b}} \int_{RR_{SR,b}} Q_{SR}(t)dt \tag{15}$$

$$Q_{AF,b} = \frac{1}{RR_{AF,b}} \int_{RR_{AF,b}} Q_{AF}(t)dt \tag{16}$$

Subscript b indicates the bth mean flow rate obtained from the bth cardiac cycle. A set of 9 beat-to-beat distributions of flow rate variables $Q_{SR,b}$ and $Q_{AF,b}$ was collected for each cardiac rhythm. Mean values, $\overline{Q_{SR}}$ and $\overline{Q_{AF}}$, were calculated from these distributions as:

$$\overline{Q_{SR}} = \frac{1}{N_B} \sum_{b=1}^{N_B} Q_{SR,b} \tag{17}$$

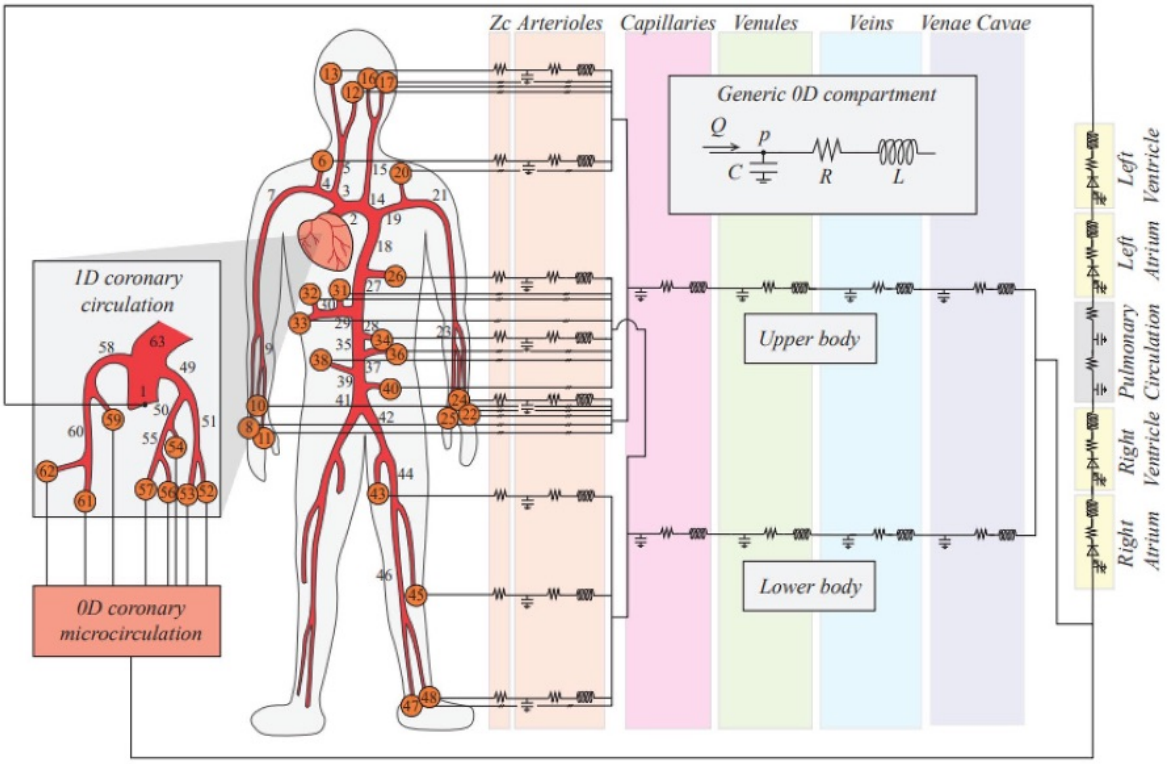

Figure 9: Multiscale illustration of the overall closed-loop model, with emphasis onto the coronary circulation (in the left side panel). For symmetry reasons, lower body 1D arteries were modeled for one leg only, but their contribution was doubled to account also for the other leg. Parameter setting can be found in [8, 7]

$$\overline{Q_{AF}} = \frac{1}{N_B}\sum_{b=1}^{N_B} Q_{AF,b} \tag{18}$$

Then, following both an inter-layer and an inter-frequency approach variations of mean value $\overline{Q_{AF}}/\overline{Q_{SR}}$ ratios were evaluated. Significance of all results was proved through statistical tests of hypothesis. Comparison between $\overline{Q_{AF}}$ and $\overline{Q_{SR}}$ was assessed via Wilcoxon's test for medians, for all cardiac layers and frequencies, as well as across layers and among frequencies under a given cardiac rhythm. ANOVA tests were also performed on $Q_{AF,b}/\overline{Q_{SR}}$ distributions, across layers and among frequencies. Simulations and statistical analyses were carried out through software MATLAB R2020b.

4.2. Result

The main findings of the present computational analysis, based on a 1D-0D multiscale model of the entire human cardiovascular system enriched by a detailed mathematical modeling of the coronary arteries and their downstream microcirculatory districts, are the following: At each simulated ventricular rate, independently from the myocardial layer, $\overline{Q_{AF}}$ was significantly reduced compared to $\overline{Q_{SR}}$. Figure 10 shows, for each coronary district, the $\overline{Q_{AF}}/\overline{Q_{SR}}$ ratio across cardiac layers for the investigated ventricular rates. Inter-layer analysis showed that $\overline{Q_{AF}}/\overline{Q_{SR}}$ progressively decreased from the epicardial to the endocardial layer in both distal LAD and LCx districts. Focusing on inter-frequency analysis, $\overline{Q_{AF}}/\overline{Q_{SR}}$ progressively worsened. In fact, they found a significant decrease in $\overline{Q_{AF}}/\overline{Q_{SR}}$ evaluated at cardiac layer when comparing the different ventricular rates.

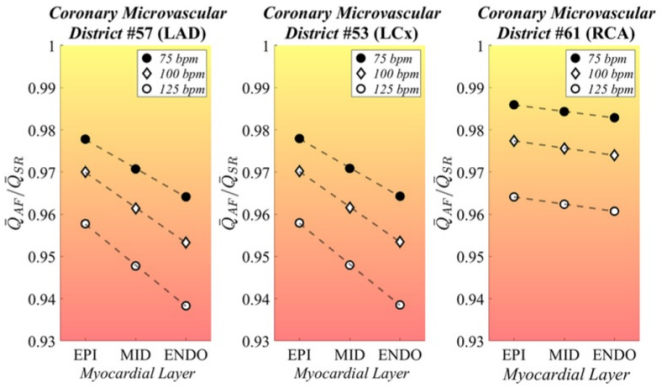

Figure 10: Dot plot reporting QAF/QSR at each simulated frequency across the myocardial layers, in three exemplificative coronary microvascular districts. Rate-specific regression lines (dashed lines) are also reported. LAD left anterior descending artery, EPI subepicardium, MID midwall, ENDO subendocardium, LCx left circumflex artery, RCA right coronary artery. [27]

So it can be said: AF exerts direct hemodynamics consequences on the coronary microcirculation, particularly at high ventricular rates, if superimposed on a susceptible substrate, Considering a constant mean ventricular rate, AF, compared to SR, decreased the mean blood flow at each myocardial layer (particularly in the ENDO layer); Given a specific myocardial

layer, higher ventricular rates during AF relate to a more pronounced reduction in microvascular blood flow, if compared to the corresponding SR simulation.

The computational framework is able to describe AF-induced direct hemodynamic effects and also details regarding the possible mechanisms behind these phenomena. In fact, an analysis of aortic pressure and left ventricular end-diastolic pressure suggests that: the reduced coronary flow during AF, compared to SR, at higher ventricular rates correlates to a drop in mean aortic pressure, the greater reduction in subendocardial perfusion, relative to the other cardiac layers, during AF in the left-sided coronary arteries (LAD and LCx) correlates to a significantly increased left ventricular end diastolic pressure.

5. Conclusions

In the present review, we have shown that arrhythmias can promote relevant changes in coronary hemodynamics. For this purpose, we first analysed the coronary model of Mynard et al. (2014) [23], which proposed a classical, anatomically based and highly detailed 1D model for the left coronary circulation (LAD and Cx) with viscoelastic wall correction and a 0D model for each intramyocardial microvascular bed downstream of each 1D coronary artery. The 0D model also took into account autoregulatory mechanisms related to intramyocardial pressure and myocardial filling. The main limitations of this model are related to simplifying assumptions. The geometry of the arterial network of the 1D channel was based on human data with a coarse coronary anatomy similar to that of sheep and therefore did not take into account anatomical differences between species or subjects. Furthermore, the 1D model did not account for the effects of vessel constriction, tethering or translational motion. The use of a 0D microcirculatory model neglected the effects of wave propagation in small vessels. The calculation of intramyocardial pressure did not take into account the effect of different myocardial stiffness (elastance) on the transmission of LV cavity pressure to the cardiac wall. Validation was limited to a single position (the proximal Cx), although general agreement with published data was noted. Before looking at the various applications, we moved on to the model of Mynard (2015) [24], which combined the coronary modelling of their initial study with the whole circulation, with the aim of making this model useful for the study of cardiovascular disease. For this reason, subsequent applications took advantage of whole circulation modelling to study the effects of ventricular fibrillation on the coronary circulation. We have seen the model of Scarsoglio et al. [28], who applied Mynard's model [23, 24] to use a simplified computational model that was able to infer how the coronary circulation responds in the presence of AF and therefore irregular beats at different ventricular frequencies. Although they achieved their goal, their model has limitations. The first limitation is that it only considers healthy patients, without taking into account the possibility of other pathologies. In fact, the model does not take into account the viscoelasticity of the heart vessels or the rate of deformation of the heart muscle, which are important markers of heart disease. In addition, the model is open-loop and considers only the left ventricle and the arterial tree, neglecting any haemodynamic feedback from systemic baroreceptor mechanisms. These latter limitations were overcome by the model of Saglietto et al. [27], who no longer considered an open model but a closed 1D - 0D model of the entire human cardiovascular system. In fact, they closed the system with a 0D representation of the arteries and veins of the pulmonary circulation. They also considered all four cardiac chambers, not just the left ventricle, and added a short-term baro-flex control mechanism that takes into account the inotropic effect of both ventricles and the control of the systemic vasculature. In the first study, despite several limitations, they were able to show that atrial fibrillation can cause a direct change in epicardial coronary flow and an imbalance in oxygen supply and demand. In the second study, they were even able to demonstrate the detrimental effects of an irregular and unrhythmic rhythm on coronary microvascular flow, which can lead to a reduction in myocardial blood flow, particularly at the subendocardial level. Despite all the limitations of the first study [28], which were overcome by the second one, It can also see here a failure to take into account possible pre-existing pathologies and the potential effects of rate control drugs. However, it must be said that the aim of the study [27] was to assess the haemodynamic effect of AF, not mediated by dysfunction, which they were able to demonstrate. It can therefore say that the 1D-0D models are models that represent a good compromise between computational cost, level of haemodynamic detail and reliability of results. They have demonstrated their suitability for studying the effects of atrial fibrillation on the coronary circulation, making it possible to study the regulation of coronary flow.

In conclusion, computational modeling can provide valuable insights for clinical practice and better guide further necessary in vivo investigations. Given the frequent coexistence of AF with other cardiac conditions, such as coronary artery disease and heart failure, and the substantial lack of computational studies considering the concurrent presence of multiple cardiac pathologies and medication intake, future modeling efforts should be focused on exploring to what extent the interaction between AF and other cardiac diseases affects coronary circulation.

References

[1] Alastruey, J., Passerini, T., Formaggia, L. and Peiró, J. [2012], 'Physical determining factors of the arterial pulse waveform: theoretical analysis and calculation using the 1-d formulation', *Journal of Engineering Mathematics* **77**, 19–37.

[2] Algranati, D., Kassab, G. S. and Lanir, Y. [2010], 'Mechanisms of myocardium-coronary vessel interaction', *American Journal of Physiology-Heart and Circulatory Physiology* **298**(3), H861–H873.

[3] Bruinsma, P., Arts, T., Dankelman, J. and Spaan, J. [1988], 'Model of the coronary circulation based on pressure dependence of coronary resistance and compliance', *Basic research in cardiology* **83**, 510–524.

[4] Dodge Jr, J. T., Brown, B. G., Bolson, E. L. and Dodge, H. T. [1992], 'Lumen diameter of normal human coronary arteries. influence of age, sex, anatomic variation, and left ventricular hypertrophy or dilation.', *Circulation* **86**(1), 232–246.

[5] Formaggia, L., Lamponi, D. and Quarteroni, A. [2003], 'One-dimensional models for blood flow in arteries', *Journal of engineering mathematics* **47**, 251–276.

[6] Frink, R. and Merrick, B. [1974], 'The sheep heart: Coronary and conduction system anatomy with special reference to the presence of an os cordis', *The Anatomical Record* **179**(2), 189–199.

[7] Gallo, C., Olbers, J., Ridolfi, L., Scarsoglio, S. and Witt, N. [2021], 'Testing a patient-specific in-silico model to noninvasively estimate central blood pressure', *Cardiovascular Engineering and Technology* **12**, 144–157.

[8] Gallo, C., Ridolfi, L. and Scarsoglio, S. [2020], 'Cardiovascular deconditioning during long-term spaceflight through multiscale modeling', *npj Microgravity* **6**(1), 27.

[9] Guala, A., Camporeale, C. and Ridolfi, L. [2015], 'Compensatory effect between aortic stiffening and remodelling during ageing', *PloS one* **10**(10), e0139211.

[10] Guala, A., Camporeale, C., Tosello, F., Canuto, C. and Ridolfi, L. [2015], 'Modelling and subject-specific validation of the heart-arterial tree system', *Annals of biomedical engineering* **43**, 222–237.

[11] Guala, A., Scalseggi, M. and Ridolfi, L. [2017], 'Coronary fluid mechanics in an ageing cardiovascular system', *Meccanica* **52**, 503–514.

[12] Hennig, T., Maass, P., Hayano, J. and Heinrichs, S. [2006], 'Exponential distribution of long heart beat intervals during atrial fibrillation and their relevance for white noise behaviour in power spectrum', *Journal of biological physics* **32**, 383–392.

[13] Hudsmith, L. E., Petersen, S. E., Francis, J. M., Robson, M. D. and Neubauer, S. [2005], 'Normal human left and right ventricular and left atrial dimensions using steady state free precession magnetic resonance imaging', *Journal of cardiovascular magnetic resonance* **7**(5), 775–782.

[14] Kochiadakis, G. E. and Kallergis, E. M. [2012], 'Impact of atrial fibrillation on coronary blood flow: a systematic review', *Journal of Atrial Fibrillation* **5**(3).

[15] Koeppen, B. M. and Stanton, B. A. [2009], *Berne & levy physiology, updated edition E-book*, Elsevier Health Sciences.

[16] Kornej, J., Börschel, C. S., Benjamin, E. J. and Schnabel, R. B. [2020], 'Epidemiology of atrial fibrillation in the 21st century: novel methods and new insights', *Circulation research* **127**(1), 4–20.

[17] Lee, J. and Smith, N. P. [2012], 'The multi-scale modelling of coronary blood flow', *Annals of biomedical engineering* **40**, 2399–2413.

[18] Luo, C., Wang, L., Feng, C., Zhang, W., Huang, Z., Hao, Y., Tang, A. and Gao, X. [2014], 'Predictive value of coronary blood flow for future cardiovascular events in patients with atrial fibrillation', *International Journal of Cardiology* **177**(2), 545–547.

[19] Martin, R. and Bates, M. [2017], 'Management of atrial fibrillation and concomitant coronary artery disease', *Continuing Cardiology Education* **3**(2), 47–55.

[20] Mynard, J., Davidson, M., Penny, D. and Smolich, J. [2010], 'A numerical model of neonatal pulmonary atresia with intact ventricular septum and rv-dependent coronary flow', *International Journal for Numerical Methods in Biomedical Engineering* **26**(7), 843–861.

[21] Mynard, J. and Nithiarasu, P. [2008], 'A 1d arterial blood flow model incorporating ventricular pressure, aortic valve and regional coronary flow using the locally conservative galerkin (lcg) method', *Communications in numerical methods in engineering* **24**(5), 367–417.

[22] Mynard, J. P. [2011], Computer modelling and wave intensity analysis of perinatal cardiovascular function and dysfunction, PhD thesis, University of Melbourne, Department of Paediatrics.

[23] Mynard, J. P., Penny, D. J. and Smolich, J. J. [2014], 'Scalability and in vivo validation of a multiscale numerical model of the left coronary circulation', *American Journal of Physiology-Heart and Circulatory Physiology* **306**(4), H517–H528.

[24] Mynard, J. P. and Smolich, J. J. [2015], 'One-dimensional haemodynamic modeling and wave dynamics in the entire adult circulation', *Annals of biomedical engineering* **43**, 1443–1460.

[25] Olufsen, M. S. [1999], 'Structured tree outflow condition for blood flow in larger systemic arteries', *American journal of physiology-Heart and circulatory physiology* **276**(1), H257–H268.

[26] Quarteroni, A., Manzoni, A. and Vergara, C. [2017], 'The cardiovascular system: mathematical modelling, numerical algorithms and clinical applications', *Acta Numerica* **26**, 365–590.

[27] Saglietto, A., Fois, M., Ridolfi, L., De Ferrari, G. M., Anselmino, M. and Scarsoglio, S. [2022], 'A computational analysis of atrial fibrillation effects on coronary perfusion across the different myocardial layers', *Scientific reports* **12**(1), 841.

[28] Scarsoglio, S., Gallo, C., Saglietto, A., Ridolfi, L. and Anselmino, M. [2019], 'Impaired coronary blood flow at higher heart rates during atrial fibrillation: Investigation via multiscale modelling', *Computer Methods and Programs in Biomedicine* **175**, 95–102.

[29] Scarsoglio, S., Guala, A., Camporeale, C. and Ridolfi, L. [2014], 'Impact of atrial fibrillation on the cardiovascular system through a lumped-parameter approach', *Medical & biological engineering & computing* **52**, 905–920.

[30] Schnabel, R. B., Yin, X., Gona, P., Larson, M. G., Beiser, A. S., McManus, D. D., Newton-Cheh, C., Lubitz, S. A., Magnani, J. W., Ellinor, P. T. et al. [2015], '50 year trends in atrial fibrillation prevalence, incidence, risk factors, and mortality in the framingham heart study: a cohort study', *The Lancet* **386**(9989), 154–162.

[31] Shi, Y., Lawford, P. and Hose, R. [2011], 'Review of zero-d and 1-d models of blood flow in the cardiovascular system', *Biomedical engineering online* **10**, 1–38.

[32] Smith, N. P. [2004], 'A computational study of the interaction between coronary blood flow and myocardial mechanics', *Physiological measurement* **25**(4), 863.

[33] Spaan, J. A., Cornelissen, A. J., Chan, C., Dankelman, J. and Yin, F. C. [2000], 'Dynamics of flow, resistance, and intramural vascular volume in canine coronary circulation', *American Journal of Physiology-Heart and Circulatory Physiology* **278**(2), H383–H403.

[34] Tu, J., Inthavong, K. and Wong, K. K. L. [2015], *Computational Hemodynamics–Theory, Modelling and Applications*, Springer.